Theory of strain relaxation in heteroepitaxial systems

A. C. Schindler,[1] M. F. Gyure,[1,2] G. D. Simms,[2] D. D. Vvedensky,[1] R. E. Caflisch,[3,4] C. Connell,[3] and Erding Luo[3]

[1]*The Blackett Laboratory, Imperial College, London SW7 2BZ, United Kingdom*
[2]*HRL Laboratories LLC, 3011 Malibu Canyon Road, Malibu, California 90265*
[3]*Department of Mathematics, University of California, Los Angeles, California 90095-1555*
[4]*California NanoSystems Institute and Department of Materials Science & Engineering,*
University of California, Los Angeles, California 90095

We introduce a general approach to calculating the morphological consequences of coherent strain relaxation in heteroepitaxial thin films based on lattice statics using linear elasticity. The substrate and film are described by a simple cubic lattice of atoms with localized interactions. The boundary conditions at concave and convex corners that appear as a result of this construction, those along straight interfacial segments, and the governing equations are obtained from a variational calculation applied to a discretized form of the total elastic energy. The continuum limit of the equations and the boundary conditions along straight boundaries reproduces standard results of elasticity theory, but the boundary conditions at corners have no such analog. Our method enables us to calculate quantities such as the local strain energy density for any surface morphology once the lattice misfit and the elastic constants of the constituent materials are specified. The methodology is illustrated by examining the strain, displacement, and energies of one-dimensional strained vicinal surfaces. We discuss the effects of epilayer thickness on the energy of various step configurations and suggest that coupling between surface and substrate steps should affect the equilibration of the surface toward the bunched state.

PACS number(s): 68.55.$-$a, 68.35.Gy, 68.60.$-$p

I. INTRODUCTION

The structural and compositional integrity of heteroepitaxial films is central to the fabrication of all quantum heterostructures. The morphology of these films is determined by a number of factors, including the manner in which strain is accommodated if the materials have different lattice constants, the surface and interface energies of the materials, and any effects associated with alloying and segregation. Thermodynamic arguments based on interfacial free energies are often used to provide a classification scheme for the *equilibrium* morphology of thin films.[1] But while such considerations undoubtedly play an important role in providing the overall driving force for the morphological evolution of thin films, they neglect a number of inherently kinetic effects. The interplay between thermodynamics and kinetics is especially germane to heteroepitaxial systems where, for example, variations in growth conditions (substrate temperature, flux, substrate misorientation) and annealing are used to manipulate the spatial and size distributions of three-dimensional (3D) coherent islands that appear during the Stranski-Krastanov growth of lattice mismatched semiconductors for quantum dot applications.[2]

Strain relaxation in heteroepitaxial systems has been the subject of an abundance of theoretical studies, but there is yet no general methodology with the versatility of the Burton-Cabrera-Frank theory,[3] rate equations,[4] or kinetic Monte Carlo simulations[5] which captures the essence of thin film evolution in the presence of lattice misfit. There are two main reasons for this. The rates of atomistic processes on strained surfaces are not determined solely by the local environment of the atoms, as in the case of homoepitaxy, but may depend on nonlocal features such as the height of a terrace above the initial substrate, the size and shape of two- and three-dimensional islands,[6,7] and their local environment.[8] This is further complicated by the competition between different strain relaxation mechanisms (e.g., alloying, misfit dislocation formation, surface profile modulations), each of which has a characteristic signature in the morphology of the substrate.[9] Additionally, any general theoretical approach must incorporate long-range elastic interactions, which are best treated within a continuum framework, and atomistic effects such as step-adatom interactions, alloying, and possibly reconstruction changes during growth.

The theoretical description of the formation of heterogeneous interfaces falls into one of three broad categories: (i) the minimization of energy functionals, including thermodynamic potentials, of various levels of sophistication to determine *equilibrium* atomic positions as a function of the lattice mismatch,[6,10,11] (ii) kinetic Monte Carlo simulations, both lattice-based[7,12] and off lattice,[13] where the hopping rules are modified to account for the effects of strain on diffusion and adatom attachment and detachment at step edges, and (iii) classical elasticity theory applied to the evolution of the growth front profile of continuous films.[14,15] These studies all require a compromise between a realistic description of interatomic interactions and the mesoscopic effects of strain relaxation due to lattice misfit.

The approach we describe in this paper is based on classical elasticity, but with the substrate and film composed of an atomistic grid, as in the method of lattice statics.[16–18] The lattice mismatch and the difference in elastic constants between the film and the substrate enter explicitly into this theory. This representation of the growing film is capable of including both atomistic and continuum elastic aspects of morphological energetics and kinetics. At the atomistic level, this includes the effect of strain on adatom diffusion,[19] and the kinetic[6,7] and thermodynamic[10,20,21] stability of islands.

Over larger length scales, there are interactions due to substrate distortion, which lead to a repulsive interaction between islands[10,22] and other surface species.[23,24] While such long-range effects are directly amenable to a description within continuum elasticity with suitably chosen materials parameters, more localized effects can be modeled with empirical or first-principles methods, especially where a direct connection between the atomistic and continuum formulations can be established.[25] Our approach can be made consistent with atomistic models cast in a valence force field representation. This allows us the flexibility to incorporate atomistic effects where needed while remaining within the general framework of linear continuum elasticity.

In this paper, we formulate the elasticity equations and boundary conditions for discrete substrates and films. In contrast to the situation for continuous films, where the boundaries are smooth curves,[14] the boundaries of our discrete systems are piecewise constant, and this requires a separate treatment. Accordingly, we derive the elasticity equations and boundary conditions from a variational calculation applied to the total elastic energy of a discretized system which respects the local symmetries of all points. The equations obtained for the interior region and along straight segments of the boundary lead, in the continuum limit, to the usual equations and boundary conditions, respectively, of linear elasticity. But at corners, the boundary conditions are best understood in quasiatomic terms as a constraint on the local displacement. We illustrate our method by calculating the interactions between steps on one-dimensional strained vicinal surfaces, which is relevant to the step-bunching instability on such surfaces. We examine qualitatively and quantitatively the strain and displacement fields that arise from the model and compare and contrast these results to known results from continuum elasticity. We also examine the influence of the thickness of the epilayer and the differences in the elastic properties between the film and the substrate and discuss the implications of these on the evolution toward the bunched state.

The outline of this paper is as follows. The basic equations of linear elasticity are reviewed briefly in Sec. II. The details of our model are then presented in Sec. III, where we describe our variational formulation of the discretized equations and boundary conditions. The complete set of equations describing the boundary conditions are compiled in the Appendix. In Sec. IV we describe some results of our model including a comparison between step-step interactions in continuum elasticity and those calculated within our model. We also present results obtained from the application of our model to vicinal surfaces that are relevant to the step-bunching instability on a one-dimensional strained vicinal surface. In particular, we discuss the likely influence of epilayer thickness and lattice mismatch of the substrate and epilayer on the evolution of the film toward the bunched state. Finally, in Sec. V we summarize our results and outline future applications of our approach.

II. CLASSICAL ELASTICITY

The following discussion presumes that the system is two dimensional (i.e., that the substrate is one dimensional), but the extension to a 3D system (i.e., a two-dimensional substrate) is straightforward. Let u_k, where $k = 1,2$, denote the Cartesian components of the displacement vector. For linear elasticity in an isotropic material, the components of the strain tensor S and stress tensor T are given in terms of the displacement vector by[26]

$$S_{kl} = \frac{1}{2} \left(\partial_k u_l + \partial_l u_k \right), \tag{1}$$

$$T_{kl} = \lambda \, \delta_{kl} S_{nn} + 2 \mu S_{kl}, \tag{2}$$

where $\partial_1 \equiv \partial/\partial x, \partial_2 \equiv \partial/\partial y$ and λ, μ are the Lamé constants. Repeated indices imply summation from 1 to 2. For the heteroepitaxial growth of a film with lattice constant a_f on a substrate with a lattice constant a_s, the normalized lattice mismatch is

$$\epsilon = \frac{a_f - a_s}{a_s}. \tag{3}$$

The strain tensor for the film is given by

$$S'_{kl} = \frac{1}{2} \left(\partial_l u'_k + \partial_k u'_l \right), \tag{4}$$

where the prime denotes quantities associated with the film. Using Eq. (3), S' can be expressed in terms of displacements with respect to the substrate lattice positions as

$$S'_{kl} = S_{kl} + \delta_{kl} \epsilon. \tag{5}$$

Accordingly, the corresponding stress tensor T' for the film is

$$T'_{kl} = \lambda' \, \delta_{kl} S_{nn} + \mu' S_{kl} - (2\lambda' + \mu') \delta_{kl} \epsilon. \tag{6}$$

In mechanical equilibrium the forces inside any volume Ω vanish,

$$\nabla \cdot T = 0, \tag{7}$$

and the force on the boundary $\partial\Omega$ equals the external pressure (in the absence of external tractions which in the case of vacuum is zero), leading to

$$\mathbf{n} \cdot T = 0, \tag{8}$$

where $\mathbf{n} = (n_1, n_2)$ is the vector normal to the surface. Additionally, at the interface between the film and the substrate, the normal component of the stress is continuous:

$$\mathbf{n} \cdot T = \mathbf{n} \cdot T'. \tag{9}$$

For a continuous film, Eqs. (7), (8), and (9) completely specify the distribution of stress within the system. For the purpose of the discussion in the next section, it is useful to point out here that the above boundary conditions can be derived from a variational principle applied to the total elastic energy. The elastic energy density $\mathcal{E}$ of the strained substrate is given by the tensor contraction $\frac{1}{2} S : T$. In terms of Cartesian components

$$\mathcal{E} = \frac{1}{2} S:T = \frac{1}{2} \lambda (\partial_n u_n)^2 + \frac{1}{2} \mu [(\partial_k u_l)^2 + \partial_l u_k \partial_k u_l] \quad (10)$$

so that the total elastic energy is

$$E_E = \int_\Omega \mathcal{E} \, dx. \quad (11)$$

The force balance equations and boundary conditions for each point then follow from setting the variation of the elastic energy with each of the displacements equal to zero:

$$\frac{\delta E_E}{\delta u_{kl}} = 0, \quad (12)$$

where $u_{kl} = \partial_l u_k$.

III. MODEL

In this section we describe a discrete atomistic model for strain, designed to agree with continuum elasticity in those regions where continuum theory has a natural discretization (namely, in the bulk and at straight boundaries). For our system, we have used an approach to formulating the equations of elasticity, based on lattice statics, that is especially appropriate for epitaxial systems. This methodology is explained in detail in Ref. 27. Here we outline the general structure of the method; mathematical details are included in the Appendix. The general approach is not to discretize Eq. (12) directly. Instead, we construct a discrete version of the elastic energy density Eq. (10), and then define the total energy as a sum of this energy density over lattice points

$$E_T = \Sigma_{i,j} \mathcal{E}(i,j). \quad (13)$$

At each point (i,j) of the grid, the energy contribution $\mathcal{E}(i,j)$ only involves terms from the nine point stencil (nearest and next-nearest neighbors) centered at (i,j). The energy contribution per site $\mathcal{E}(i,j)$ is written in its most general form in the Appendix, as are specific cases of interest.

The principal virtue of this formulation is that it combines atomistic and continuum approaches. If the computational grid is the same as the underlying atomistic lattice, then the discrete version of the energy may be considered purely atomistic. This correspondence is equivalent to imposition of the Cauchy-Born hypothesis, that the atomistic lattice displacement equals the macroscopic elastic displacement. The advantage of the atomistic interpretation is that it allows us to tailor the energy density to suit specific atomistic geometries where continuum elasticity fails to inform us as to what discrete equations to use. In particular, we have used it here to derive numerical boundary conditions at the sharp corners at the top of the film, and to derive equations at the film/substrate interface.

Using the discrete version of Eq. (10), the discretized force balance laws come from minimizing the total energy E_T. The resulting equations are

$$\frac{\partial E_T}{\partial u_k(i,j)} = 0, \quad (14)$$

which is the discrete analog of Eq. (12). These discrete equations are formally equivalent to discretizations of the classical elasticity equations. In particular, at interior points Eq. (14) is a discretization of Eq. (7), and at flat edges it is a discretization of Eq. (8). At corners and at material interfaces, however, these equations are new and do not admit a continuum interpretation.

The boundary conditions that arise from performing a variation on the discrete energy have the effect of regularizing the singularities that exist in continuum theory at, e.g., interior corner points. This regularization is not completely artificial; since our discretization is at the atomic scale, it is performed at the appropriate length scale. In a real material, the singularities present in continuum elasticity are, in fact, regularized by the atomic lattice. This regularization could be done in a more controlled fashion, entirely within our framework, by using an appropriately parametrized atomistic bond model for the energy at these singular points. This is beyond the scope of the present work, however, and we expect that qualitatively correct results for step equilibrium and dynamics can be obtained with the present form of the energy.

Our method for treating elasticity should be placed in context with an alternative approach,[28,29] which is based on the use of Green's functions. This approach makes use of the analytic expression for the half-space Green's function that describes the displacement at any point **x** in the bulk due to a unit force acting at another point **x**′. Then, assuming that the bulk is homogeneously strained, a multipole expansion of the force distribution caused by a step can be made. Multiplying each term in the expansion by the appropriate derivative of the Green's function, the displacement at any point due to the presence of a step can be obtained as well as the force on one step due to another. This is a powerful and appealing approach, but has several serious limitations. The use of the half-space Green's function implies not only that the epilayer is homogeneously strained, but also that the epilayer thickness is much greater than the step height. Furthermore, the distance between steps must be sufficiently large that the step interactions can be approximated by only a few terms in the multipole expansion. Finally, if the material system is inhomogeneous, then depending on the geometry and elastic parameters, the Green's function approach may be either difficult or impractical to implement.

These restrictions cause problems if the issue to be addressed is the interaction between steps on very thin epilayers on a vicinal substrate, or the interaction between islands on the first few epilayers on a singular surface. In many cases of practical interest, heteroepitaxial layers are tunnel barriers or quantum wells whose thickness is often no more than a few layers. On a vicinal surface, the presence of steps on the substrate causes the assumption of homogeneity of the epilayer strain to be violated. Even on nominally singular surfaces, the epilayers can easily be thin enough to violate the assumption that the step height is much smaller than the epilayer thickness. The initial nucleation of quantum dots is of intense interest and also occurs in a regime where the Green's function is not valid. The epilayer is thin in the nucleation phase and island distances may be small enough
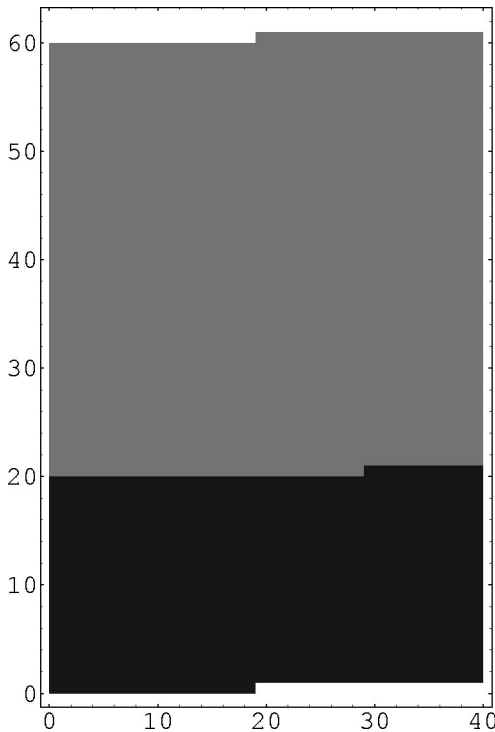
FIG. 1. A vicinal surface with a single step consisting of an epilayer of *A*-type atoms (shown in gray) on a substrate of *B*-type atoms (shown in black).

to violate the assumptions of the multipole expansion. Our approach suffers from none of these restrictions and, assuming that linear elasticity holds down to length scales of a few lattice spacings, as has been observed,[30,31] our only approximations are in the treatment of the atomistic effects relevant very near the step edges and at the surface. Even these effects can be accommodated with some additional effort as described in Sec. V.

IV. RESULTS AND DISCUSSION

As an illustration of our method, we now consider step relaxations and step-step interactions on strained vicinal surfaces.

A. Step relaxations

We begin by examining the behavior of the displacement and strain fields given by our model for steps on a strained vicinal surface. Figure 1 shows the basic geometry that will be considered. The epilayer (shown in gray) consists of 40 layers of material with isotropic elastic constants $\lambda = 1$ and $\mu = 1$ on a substrate (shown in black) of thickness 20, which also has elastic constants $\lambda = \mu = 1$. The buried step on the interface between substrate and epilayer is horizontally offset from the surface step to indicate a generic nonsymmetric configuration. Although only one step is shown, skew-periodic boundary conditions are applied so that the model describes an infinite step train, not an isolated step. The lower boundary of the lattice necessarily also has a step, to be consistent with the skew-periodic boundary conditions.

The atoms immediately on the lower boundary are held at zero displacement in all of the subsequent relaxation calculations, to approximate bulk behavior.

For clarity we will examine the effects of surface stress as a separate case from epilayer mismatch, with the knowledge that the effects can be combined if desired. For the case of epilayer misfit with no surface stress, there is a lattice mismatch of 1% between substrate and epilayer with sign such that the epilayer is under compressive strain. For the alternate case of surface stress with no epilayer misfit, the bonds between pairs of atoms on the epilayer-vacuum interface are modified to have a lattice constant 1% larger than the bulk, giving a compressive stress for the surface layer only. In the latter case, the substrate and epilayer are indistinguishable, so that the system is effectively a layer of thickness 60 with a step on the top and the bottom held at the zero-displacement bulk position.

Figure 2 shows the *x* and *y* components of displacement produced by the epilayer misfit model for this particular step configuration and Fig. 3 shows the displacements for the surface-stress only case. In Fig. 3 the coupling of the horizontal surface stress to vertical displacements is apparent. The step edge breaks the planar symmetry of the surface and allows this coupling, since the two stresses on either side of the step produce a torque about the step edge.

Better qualitative appreciation of the results of the relaxation can be gained from graphing the components of the strain tensor. Figure 4, for the compressed epilayer, clearly shows the distinct strain fields produced by the surface step and the buried interface step. The linear *y* displacement no longer dominates the image as it did in Fig. 2(b), since the strain only contains derivatives of the displacement. Of note in the figure is the different "polarity" of the *x* and *y* strains at the surface step vs. the interface step, and the structure around each of the steps as the value of the strain component oscillates between positive and negative values as a function of angle. Figure 5 shows the strains produced by surface stress only. In this case, the buried step experiences no strain, and the visible strain field is due to the surface step alone. The angular structure around the step in (a) and (c) is noticeably different from Fig. 4, suggesting more dominant higher multipole moments. In both Figs. 2 and 3, the lower boundary of the lattice is invisible since it has the same zero value of strain as the vacuum.

Having discussed some of the qualitative features of step relaxations produced by our model, we now turn to a more quantitative analysis. In particular, we wish to show that the displacements due to surface steps produced by our model are in quantitative agreement with predictions derived from continuum elastic theory in regimes where we expect the latter to be valid. The results from continuum elastic theory we will compare to are for displacements due to an isolated step; our method, however, most naturally treats periodically placed steps in a step train. In order to separate the effect of an isolated step from that of the periodic images, we perform a lattice sum of periodic multipole forces, which is then used for evaluation of the multipole coefficients due to step displacements.
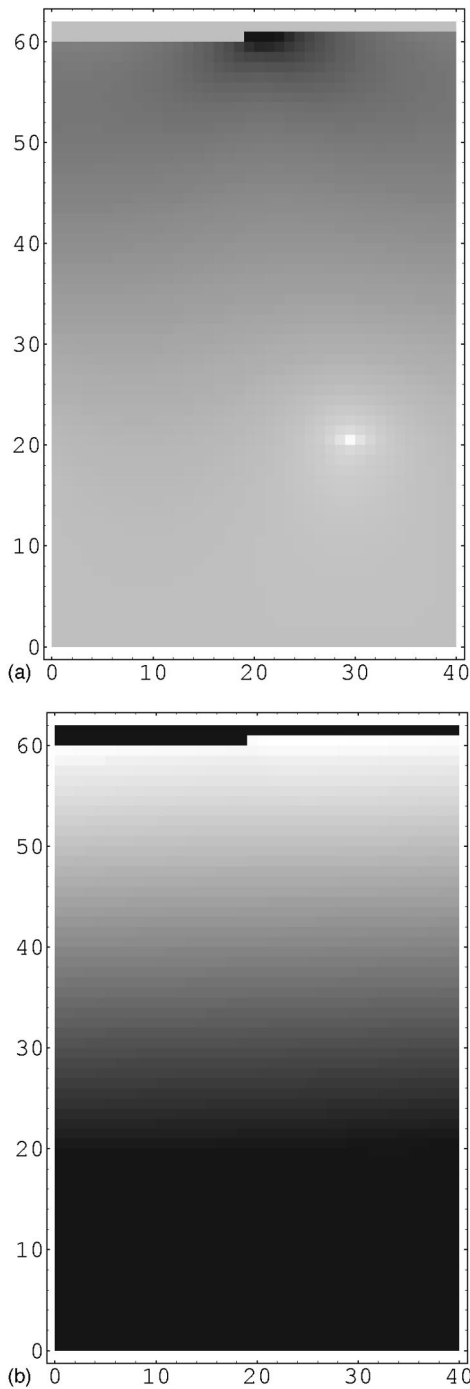
FIG. 2. Displacement fields due to the step from Fig. 1 on a compressively strained epilayer. The color of the vacuum area above and below the lattice indicates the zero of the scale, and displacements are calculated with respect to the reference lattice as described in the Appendix. The bottom-most layer of atoms is fixed at zero displacement to approximate the bulk. Lighter shading represents positive displacements and darker shading represents negative displacements. The x displacements are shown in (a) and the y displacements (with a different zero of the grayscale) are shown in (b). Because of the Poisson ratio of the material, there is an overall increasing y displacement that visibly overwhelms the details of y displacements due to the step itself.
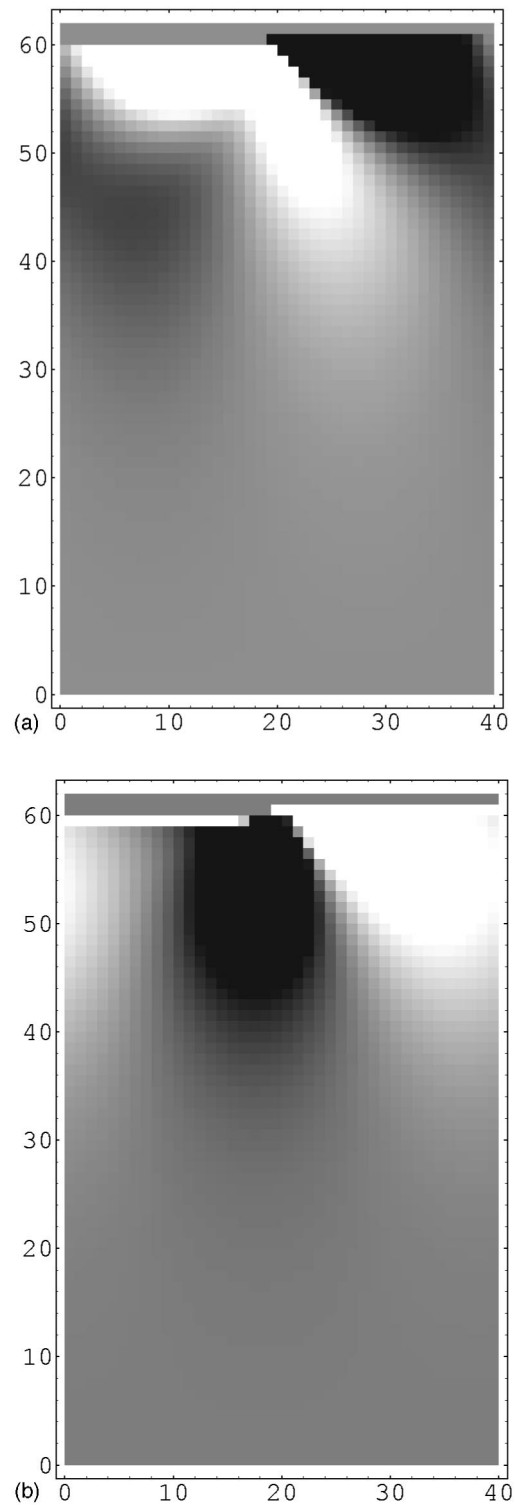

FIG. 3. Displacement fields due to the step from Fig. 1 with intrinsic surface stress in the material. The gray color in the vacuum region above and below the lattice represents the zero of the scale, with lighter shading indicating positive displacement and darker shading indicating negative displacement with respect to the reference lattice. The shading gradient is not to the same scale as Fig. 2, since the absolute displacements from this surface stress effect are smaller. The x displacements are shown in (a) and the y displacements are shown in (b).
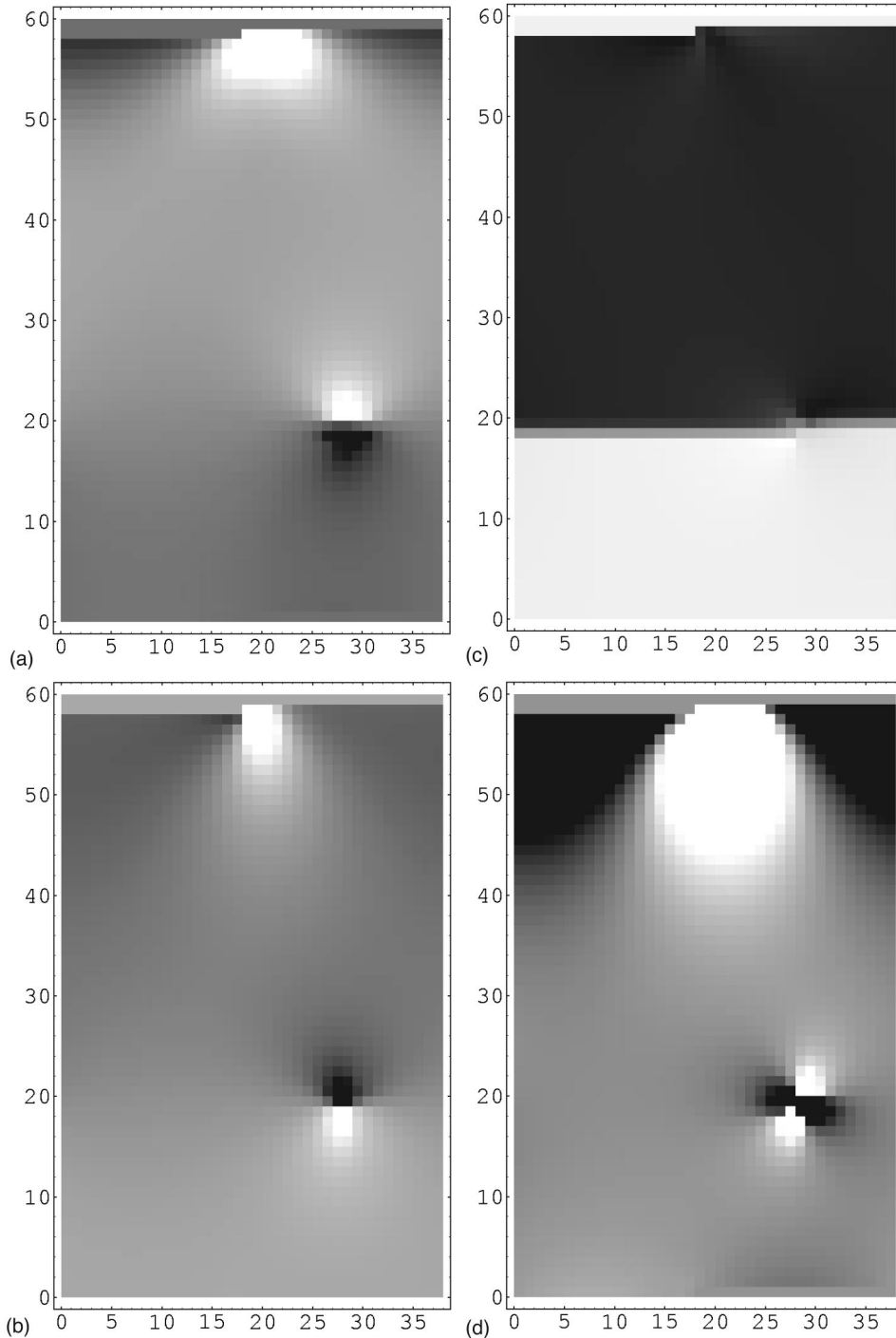
FIG. 4. Components of the strain field due to a step on a compressively strained epilayer, with the same step geometry as previous figures. In each sub-figure, the shading of the vacuum region above the lattice represents the zero of the scale, with white representing positive values and black representing negative values. The components shown are as follows: (a) xx component, (b) yy component, (c) xy component, and (d) hydrostatic strain (trace of strain tensor).

The effect of a single isolated step in an (horizontally) infinite domain is addressed by superposition in periodic boundary conditions. The computational domain, when skew-periodic boundaries are applied, is effectively infinite, and is populated by an infinite number of equally spaced steps. The distortion fields produced by each of these steps linearly superposes, however, and may be summed. For example, a one-dimensional "dipole potential" term[32] of strength m_1 for an isolated step at x_0,

$$V_1^1 = \frac{m_1}{x - x_0} \qquad (15)$$

sums as

$$V_1^\infty = \sum_{n=-\infty}^{\infty} \frac{m_1}{x - x_0 + nL} = m_1 \frac{\pi}{L} \cotan\left(\frac{\pi}{L}(x - x_0)\right), \quad (16)$$

where L is the periodicity of the system. The summed dipole force is found as the negative derivative of the potential:

$$f_1^\infty = -\frac{d}{dx} V_1^\infty = m_1 \left(\frac{\pi}{L}\right)^2 \mathrm{cosec}^2\left(\frac{\pi}{L}(x - x_0)\right). \quad (17)$$
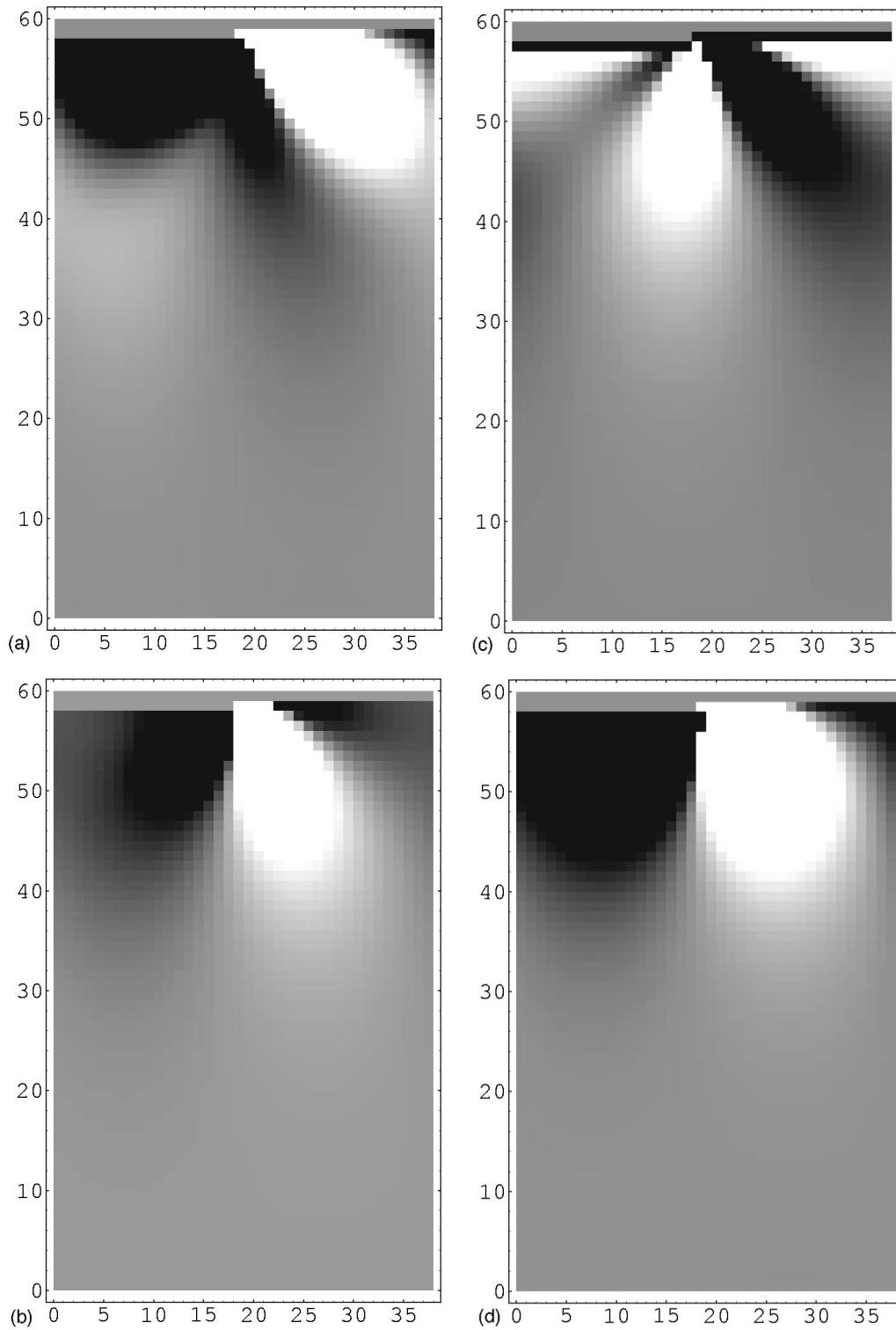
FIG. 5. Components of the strain field due to a step with intrinsic surface stress in the material. In each subfigure, the shading of the vacuum region above the lattice represents the zero of the scale, with lighter shades representing positive values and darker shades representing negative values. The components shown are as follows: (a) xx component, (b) yy component, (c) xy component, and (d) hydrostatic strain (trace of strain tensor).

x Displacements on Terrace
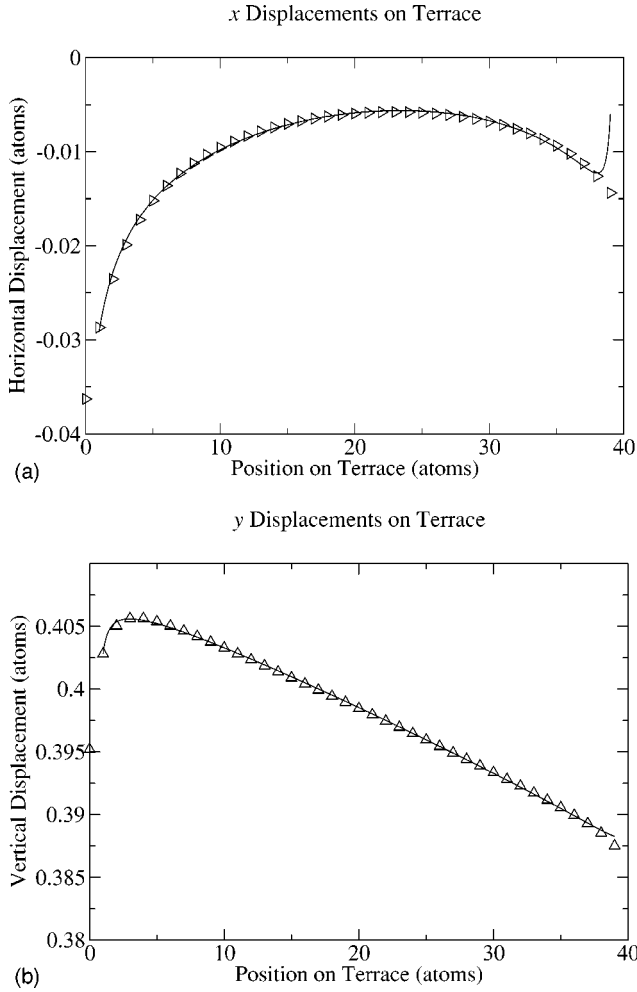

(a)

y Displacements on Terrace

(b)

FIG. 6. Displacements at the surface layer (from Fig. 2) for a strained epilayer with no surface stress. The *x* displacements (a) and *y* displacements (b) are shown as a function of position from one step to the next periodic image step. The dots are the displacements produced by the model and the solid lines are fits to the function described in the text, up to dipole order. (The first and last points are left out of the fit.)

All higher order multipole terms may be summed analogously. The single step monopole potential term

$$V_0^1 = m_0 \ln(x - x_0) \tag{18}$$

cannot be directly summed and instead the corresponding force

$$f_0^1 = -\frac{d}{dx} V_0^1 = \frac{m_0}{x - x_0} \tag{19}$$

is summed, and then integrated to give the lattice-summed monopole potential

$$V_0^\infty = m_0 \ln\left[\sin\left(\frac{\pi}{L}(x - x_0) \right) \right]. \tag{20}$$

These periodic functions are best examined on a single period extending over the *terrace* between two steps (Fig. 6),
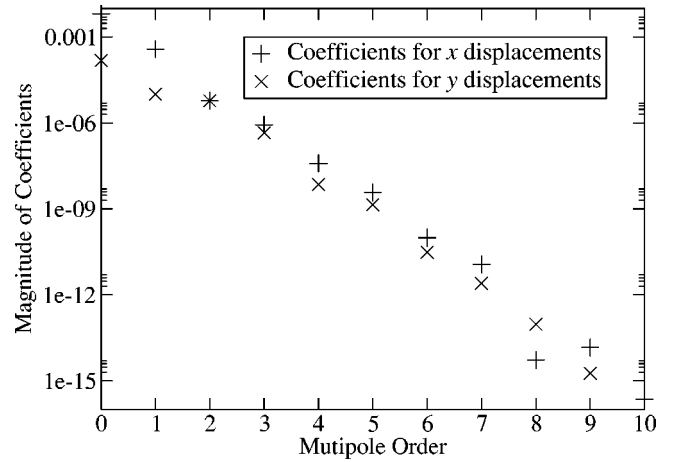

FIG. 7. Magnitude of *x* and *y* displacement multipole coefficients for first 12 multipoles $m_0 \cdots m_{11}$ for a strained epilayer with no surface stress.

and not on a domain containing a pole, which would require fitting with an infinite discontinuity between left- and right-hand sides.

The coefficients m_0, m_1, m_2, etc., of these lattice-summed terms are identical to the coefficients of the isolated step continuum multipole expansion. This allows the coefficients from a fit to our model on a terrace to be compared directly to the coefficients derived from the continuum theory for a single step.

Figure 6 shows the *x* and *y* displacements along a terrace for the case of a uniformly compressed epilayer. Included are fits to the functional form described above to dipole order. We also fit the data to a 12 term series and extract the corresponding multipole coefficients of the isolated step; these are shown in Fig. 7. We first note that the logarithmic monopole is dominant, and the falloff with increasing multipole order is rapid and uniform. The dipole coefficient, for example, is more than an order of magnitude smaller than the monopole coefficient. Dominance of the logarithmic monopole is also evidenced by the fact that using only the monopole and dipole terms results in the excellent fit shown in Fig. 6. The simplest continuum elastic theory predicts the existence of a monopole term only and should be valid in the limit of the step height small compared to the distance between steps in our model. That condition is reasonably well satified for the case shown here, hence the relative dominance of the monopole term. The existence of other multipole terms, though small, nevertheless shows that our model is capturing some of the atomistic effects that are present and therefore goes beyond a purely continuum description.

Figure 8 shows the monopole coefficient m_{0x} for the *x* component of the displacement along the surface as a function of lattice mismatch ϵ. For each ϵ, m_{0x} is calculated from the simulation data for 16 different values of the elastic parameters λ and μ. These data are compared to the theoretical prediction $m_{0x} = 2(\lambda + 2\mu)/\epsilon$, which can be derived either from continuum theory[33] or from a discrete model.[27,34] The agreement between the simulation data and the analytic expression is quite good, but not exact. This is again what we would expect since we are in a regime in which the atomistic
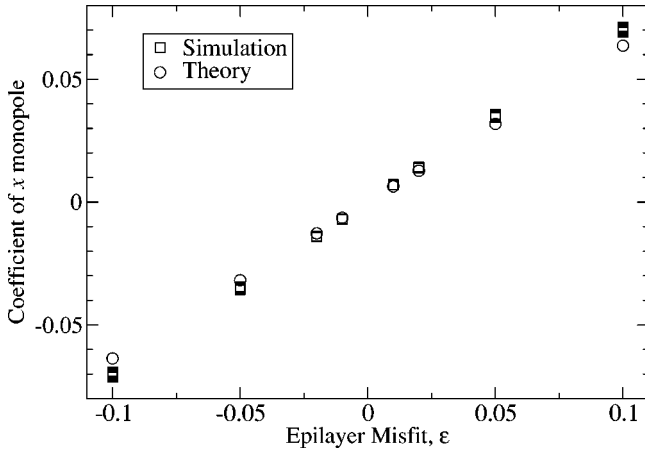
FIG. 8. Monopole coefficient m_{0x} for the x component of the displacement along the surface. Data is plotted as a function of lattice misfit ϵ for 128 values of elastic coefficients λ, μ, and ϵ. Values from the simulation ($\square$) and from theory ($\bigcirc$) are plotted.

effects captured by our discrete model are small, but not completely negligible. Thus, we have shown from this and the preceding data that our model reproduces the expected continuum results in the approriate limit, but with corrections due to the discrete nature of the model that may be important in other regimes.

B. Step-step interaction energy

We now turn our attention to the interaction energy between steps produced by our model. For a general linear elastic material with a stepped surface, there are forces between steps even in the absence of misfit strain. In the Green's function approach discussed above, these forces separate (conceptually) into two types: a repulsive "dipole" interaction,[33] which is due to the intrinsic surface stress of the steps, and a logarithmic repulsion between inequivalent steps in the form of a force "monopole,"[35,36] which is due to the elastic distortion of the surface.

In a film under an externally imposed strain, such as that derived from coherent epitaxy to a lattice-mismatched substrate material, there is an additional, attractive interaction between steps due to a force "monopole"[36] which is logarithmic. The unstrained monopole force of the previous paragraph is fundamentally different from this strained monopole, in that the presence or absence of the former depends on relative step orientations, while the latter is present for all steps. In the calculations described below, all steps face the same direction, obviating any repulsive monopole.

The force f_m on a single step at position x_m is approximated, to dipole order, by[26,28,33]

$$f_m = \sum_{\substack{n \\ n \neq m}} \left(\frac{\alpha_1}{(x_n - x_m)} - \frac{\alpha_2}{(x_n - x_m)^3} \right), \qquad (21)$$

where α_1 is determined by the elastic constants of the materials and the lattice mismatch, and α_2 is determined by the elastic constants of the epilayer material and the intrinsic surface stresses.
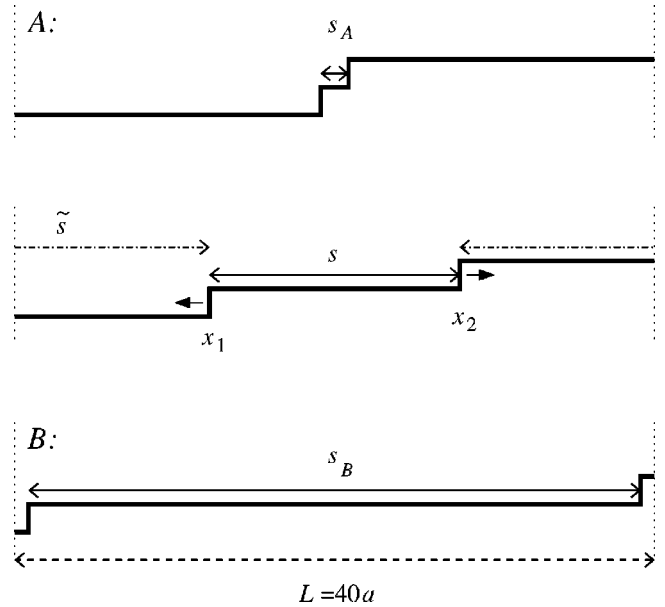

FIG. 9. Geometry used for calculating two-step interaction energy. Left and right boundaries are skew periodic. Steps are moved from configuration A to configuration B in such a way that the total area remains constant (mass is conserved).

In light of the above discussion, we now compare the elastic energy due to step-step interaction obtained in our model to the predicted interaction. To calculate the total elastic energy as a function of step distance, we use the geometry shown in Fig. 9, with skew periodic boundary conditions as appropriate for modeling an infinite step train. The two steps are moved by equal amounts in opposite directions to conserve the mass of the system, thereby preventing the uncontrolled introduction of "background" bulk elastic energy in the process. With the steps at each lattice position between configurations A and B, we record the total elastic energy.

We expect that the relevant quantities determining the qualitative behavior of the system are μ_i/λ_i and μ_s/μ_e, where the subscripts s and e are for substrate and epilayer properties, and $i \in \{s,e\}$. Every property that depends on lattice mismatch ϵ does so linearly, so that scales out as well. For simplicity we calculate with $\lambda = \mu = 1$, and $\epsilon = 1\%$. For Si, $\mu/\lambda \approx 1.1$; for Ge, $\mu/\lambda \approx 1.2$, and $\mu_{Si}/\mu_{Ge} \approx 1.2$, so the qualitative results should hold for that physical system and others with similar scaled elastic properties. In this computation, the grid spacing was chosen such that each atomic lattice spacing is one numerical grid point across. The system has a lateral size of 40 lattice spacings, which would be equivalent to a physical size of approximately 22 nm for a Si/Ge system.

The first case we consider has an epilayer thickness of 30 ML, large enough that we expect this case to behave as if the epilayer were uniformly strained. The results for the total energy as a function of step separation are shown by the square data points in Fig. 10. The agreement between the data from our model and the solid line is excellent, indicating that our model reproduces the expected logarithmic interaction between steps on a homogeneously strained epilayer at distances larger than one atom.
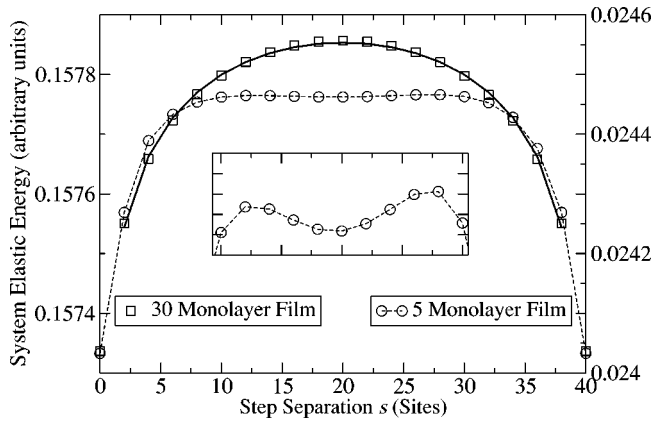
FIG. 10. Total system energy for a step moving from configuration A ($s=0$) to configuration B ($s=20$), for both a 30 atom thick epilayer (squares, left axis) and a 5 atom thick epilayer (circles, right axis). Both calculations are on a 30-layer substrate. The solid line is a logarithmic fit to the thick epilayer data, and the inset is the central portion of the thin epilayer data with 20× vertical exaggeration.

The circle data points in Fig. 10 show the total elastic energy for an epilayer thickness of only 5 ML. Note that the behavior is qualitatively different than the thick epilayer case. There is a "dip" in the energy as the surface steps pass over the terrace midway between configurations A and B. This local minimum in energy becomes more pronounced for epilayers thinner than 5 monolayers. Figure 11 shows the hydrostatic strains for two of the configurations whose energies are plotted in the preceding figure. Note that there is significant elastic interaction between the epilayer steps and subsurface features at the epilayer-substrate interface. This interaction is what leads to the local minimum in energy when the epilayer steps are moved with respect to the buried steps, and is an effect not present in models assuming a homogeneously strained epilayer. In fact, this effect would be very difficult to capture with any Green's function-based approach.

We expect this to have considerable implications for the dynamics of step bunching. Although only metastable, step configurations that experience significant coupling to the substrate may be expected to slow or even completely suppress the step bunching phenomenon normally expected on vicinal surfaces even under annealing conditions. A full investigation of step dynamics using this elastic model coupled to an equilibrium model for step dynamics[28] is in progress will be reported on elsewhere.

V. SUMMARY AND FUTURE APPLICATIONS

We have presented a new method to study the influence of elastic interactions in strained one-dimensional systems using an approach based on lattice statics using linear elasticity theory. An application is the problem of step relaxations and step-step interactions on vicinal surfaces. We have examined in detail the behavior of our model for this particular problem and found the step relaxations to be consistent with the predictions of continuum elastic theory in the limit where the

continuum theory would be expected to hold (the thick epilayer limit). We have also demonstrated, however, that the discrete nature of the model allows us to capture many effects that are essentially atomistic in nature. When considering step-step interactions, we found that there is a significant influence of perturbations of the elastic field on the surface due to buried substrate morphologies. These may well lead to long relaxation times for very thin epilayers, where the actual critical thickness depends on the misfit ϵ as well as on the elastic constants of the two involved materials. Upon increase of the epilayer thickness, we observe a decay of the substrate influence until at epilayer heights of roughly 30–50 monolayers the effects of the initial substrate configuration vanish.

We expect this general methodology to have wide applicability to problems involving strain in epitaxial growth. Here, the method was formulated for a simple cubic lattice in 2D, but it is easily extendible to noncubic lattices and 3D. In addition, the atomistic nature of our formulation makes it applicable to including surface and step edge effects, provided that a suitable description of the local energy at these sites is available. At the atomistic level, our model is an example of a valence force field model. Valence force field models, such as the Keating model, have been validated for bulk elastic properties of many real materials.[37–39] Valence force field models accurately describing the energy of atomic configurations at surfaces and step edges are not generally available, but there are no fundamental obstacles to developing and validating such models.

One of the main motivations for this work is our intention of incorporating elastic effects into the level-set method[40] for describing the morphological evolution of epitaxial films.[41] This technique is based on the representation of the moving growth front (the step edges) in terms of an auxiliary function (the level set function) which permits a straightforward solution of the associated Stefan problem and handles in a natural way the topological changes associated with the nucleation of islands and their coalescence. By treating the x-y variables as continuous, but the z direction as discrete, this method is ideally suited both to coupling continuous fields to island motion and to describing abrupt atomistic effects associated with the initial stages of heteroepitaxial growth, such as the 2D-3D transition during Stranski-Krastanov growth.[42] The coupling of the adatom diffusion field to island-boundary motion has already been accomplished,[43] so we now turn to the effect of elasticity on the motion of island boundaries.

The new method opens up a vast field of possible applications. Beginning with the most fundamental aspects of growth, we can examine the effect of strain on adatom hopping,[44] nucleation, and island stability,[45] as well as investigate the issue of kinetic versus equilibrium effects in the island statistics.[46,47] These factors, in turn, impact upon the extent of lateral[2] and vertical ordering[48,49] of 2D and 3D islands. Growth phenomena on patterned substrates is also easily within the scope of this method.[50]
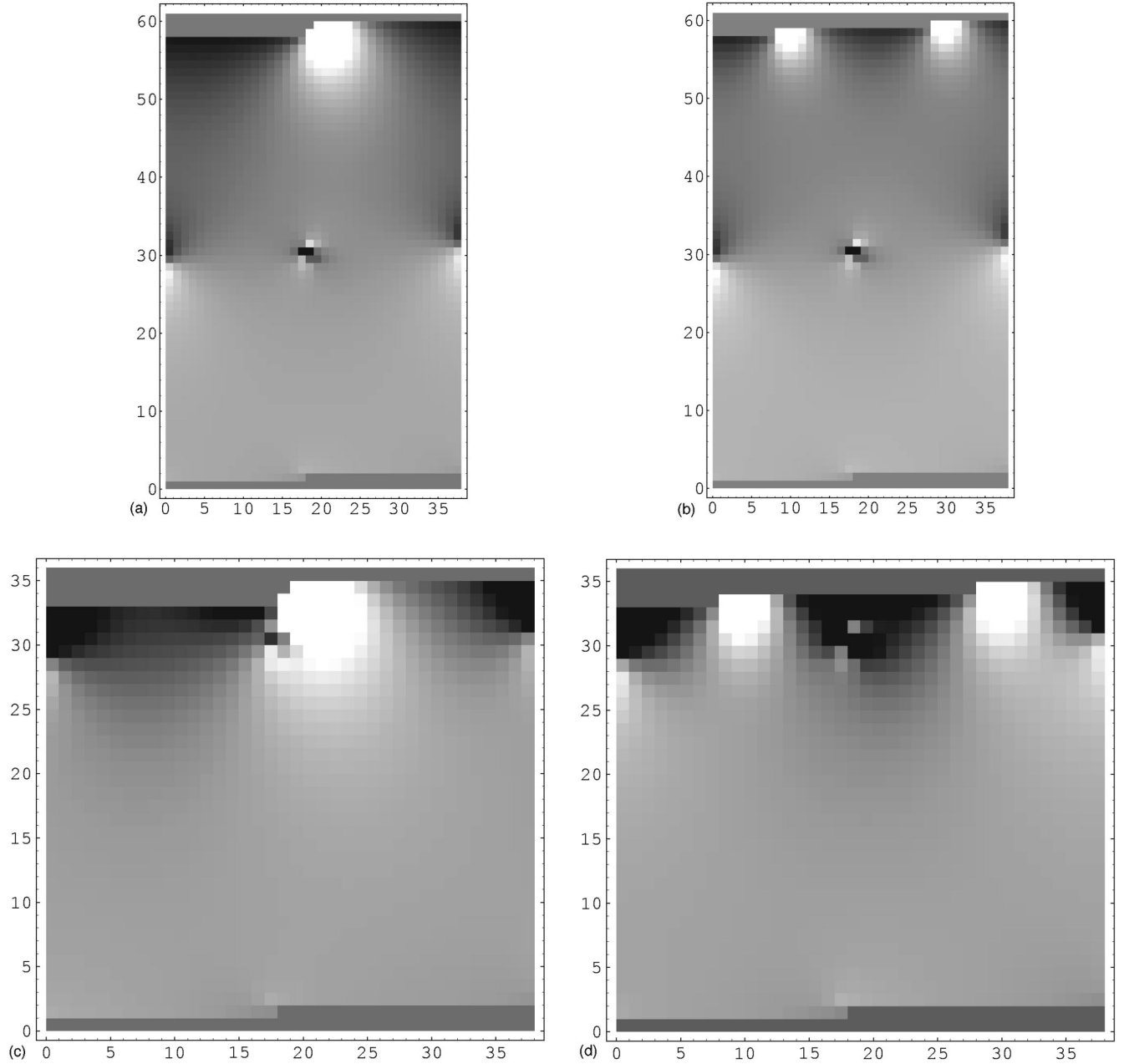
FIG. 11. Hydrostatic strain for sample configurations from the Fig. 10 calculation. The top two subfigures (a), (b) are a 30-monolayer film and the bottom subfigures (c), (d) are a 5-monolayer film. The subfigures on the left (a), (c) are for $s=0$ and those on the right (b), (d) are for $s=L/2=20$.

APPENDIX: ELASTIC ENERGY

For a two-dimensional cubic lattice with lattice constant h and lattice coordinates $\boldsymbol{i}=(i_1,i_2)$, denote the reference position as $\boldsymbol{x}=(x_1,x_2)$, the elastically deformed position as $\boldsymbol{X}=(X_1,X_2)$, and the displacement as $\boldsymbol{u}=(u_1,u_2)=\boldsymbol{X}-\boldsymbol{x}$. De-

fine the translation operators $T_k^{\pm}$ and finite-difference operators $D_k^{\pm},D_k^0$ as follows:

$$T_k^{\pm}f(\boldsymbol{i})=f(\boldsymbol{i}\pm\mathbf{e}_k), \tag{A1}$$

$$D_k^+f(\boldsymbol{i})=h^{-1}(T_k^+-1)f(\boldsymbol{i}),$$

$$D_k^-f(\boldsymbol{i})=h^{-1}(1-T_k^-)f(\boldsymbol{i}), \tag{A2}$$

$$D_k^0f(\boldsymbol{i})=(2h)^{-1}(T_k^+-T_k^-)f(\boldsymbol{i}),$$

in which $\mathbf{e}_k$ is the unit vector in the kth direction for $k=1,2$. Define the bond displacement $\mathbf{d}^{k\pm}$ at the point $\boldsymbol{i}$ as

$$\mathbf{d}^{k\pm}(\boldsymbol{i})=(d_1^{k\pm},d_2^{k\pm})=D_k^{\pm}\boldsymbol{u}(\boldsymbol{i})-\epsilon\mathbf{e}_k. \tag{A3}$$

As discussed in Sec. II, the lattice mismatch parameter ϵ in the epilayer is the relative difference between the equilibrium lattice constant and the lattice constant imposed on the epilayer by the substrate.

The discrete strain components at a point $\boldsymbol{i}$ are defined as

$$S_{kk}^{\pm}=d_k^{k\pm},$$

$$S_{kl}^{pq}=(d_k^{lq}+d_l^{kp})/2 \tag{A4}$$

in which the values of k and l are 1 or 2 and the values of p and q are $+$ or $-$. The strain component $S_{kk}^{\pm}$ corresponds to a bond in the $\pm\mathbf{e}_k$ direction from the point $\boldsymbol{i}$; the component S_{kl}^{pq} corresponds to two interacting orthogonal bonds in the $p\mathbf{e}_k$ and $q\mathbf{e}_l$ directions from the point $\boldsymbol{i}$.

1. Micromechanical model

The elastic energy used here has a micromechanical interpretation as consisting of nearest neighbor springs, diagonal springs, and bond bending terms. For nearest neighbor linear springs and linearized bond bending springs, in which the spring constants are a and b, respectively, the energy at a point is

$$E_{nnbb}=\frac{1}{2}\,a\sum_{p=\pm,k=1,2}(S_{kk}^p)^2+\frac{1}{2}\,b\sum_{p=\pm,q=\pm}(S_{12}^{pq})^2. \tag{A5}$$

In order to retain maximal locality, we use "virtual" diagonal spring with spring constant c, defined for example between a point $(0,0)$ and the average of its nearest neighbors $(1,0)$ and $(0,1)$, for which the energy is

$$E^{++}=\frac{1}{2}\,c(\mathbf{e}_1+\mathbf{e}_2)\cdot\left\{[\boldsymbol{u}(1,0)+\boldsymbol{u}(0,1)]\Big/2-\boldsymbol{u}(0,0)\right\}^2$$

$$=c(S_{11}^++S_{22}^++2S_{12}^{++})^2/8. \tag{A6}$$

More generally for $p=\pm,q=\pm$ define

$$E^{pq}=c(S_{11}^p+S_{22}^q+2pqS_{12}^{pq})^2/8. \tag{A7}$$

The energy density E is a combination of these four virtual diagonal springs; i.e.,

$$E=\sum_{p=\pm,q=\pm}E^{pq}. \tag{A8}$$

Add and rearrange Eqs. (A5) and (A8), to obtain the resulting energy

$$E=\alpha\sum_{p=\pm,k=1,2}(S_{kk}^p)^2+\sum_{p=\pm,q=\pm}\{2\beta(S_{12}^{pq})^2+\gamma S_{11}^pS_{22}^q\} \tag{A9}$$

in which

$$\alpha=(a+c)/2=C_{11}/4,$$

$$\beta=(b+c)/2=C_{44}/4,$$

$$\gamma=c/8=C_{12}/4, \tag{A10}$$

and C_{ij} are the Voigt constants. The energy density (A9) is the discrete analogue of the continuum energy for elasticity with cubic symmetry. For isotropic elasticity, as in Sec. II, the coefficients should be chosen as

$$\alpha=(\lambda+2\mu)/4,$$

$$\beta=\mu/4,$$

$$\gamma=\lambda/4, \tag{A11}$$

i.e., $a=\mu-\lambda$, $b=\mu/2-2\lambda$, $c=2\lambda$.

The discrete energy density (A9) has been chosen to be maximally localized; so that the energy density E at a point $\boldsymbol{i}$ is a quadratic function of displacement $\boldsymbol{u}$ at the five point stencil consisting of the point $\boldsymbol{i}$ and its nearest neighbors, and the corresponding force balance equations involve only the nine point stencil consisting of the point $\boldsymbol{i}$ and its nearest and next-nearest neighbors.

2. Interfaces

For problems in which the underlying lattice has cubic symmetry but the material geometry includes interfaces, we generalize the energy in Eq. (A9) by only keeping bond interactions that are consistent with cubic symmetry but not imposing a symmetry constraint on the strength of the interactions. The resulting energy has the form

$$E=\sum_{p=\pm,k=1,2}\alpha_k^p(S_{kk}^p)^2+\sum_{p=\pm,q=\pm}\beta^{pq}(S_{12}^{pq})^2+\gamma^{pq}S_{11}^pS_{22}^q. \tag{A12}$$

Each coefficient α_k^p, as well as the lattice mismatch parameter ϵ, corresponds to a bond between two atoms; each of the coefficients β^{pq} and γ^{pq} corresponds to the interaction of two bonds in orthogonal directions from a central point, which defines a square "cell." We assume that the values of $\alpha_k^{\pm}$ and ϵ (β^{pq} and γ^{pq}) depend only on the material type of the two (four) atoms at the endpoints of the corresponding bond (cell).

Consider a system consisting of two materials with elastic parameters $\alpha^m,\beta^m,\gamma^m,\epsilon^m$ for $m=1,2$. Denote a cell or bond to be "pure" if all of its vertices are of a single material type and "mixed" otherwise. For maximal simplicity, we make the following assumptions, which could easily be generalized.

(1) For pure bonds (pure cells) in material m, $\alpha_k^p=\alpha^m$ and $\epsilon=\epsilon^m$, ($\beta^{pq}=\beta^m$ and $\gamma^{pq}=\gamma^m$).

(2) For mixed bonds (mixed cells) in a two-material system, $\alpha_k^p=\frac{1}{2}(\alpha^1+\alpha^2)$ and $\epsilon=\frac{1}{2}(\epsilon^1+\epsilon^2)$ [$\beta^{pq}=\frac{1}{2}(\beta^1+\beta^2)$ and $\gamma^{pq}=\frac{1}{2}(\gamma^1+\gamma^2)$].

(3) For a bond (cell) in which one of the vertices is in the vacuum $\alpha_k^p=0$ ($\beta^{pq}=\gamma^{pq}=0$).

3. Force balance equations

Assumptions (1)–(3) provide an algorithm by which the elastic coefficients and elastic energy can be determined for

any material configuration involving two materials (i.e., a substrate and an epilayer) and a vacuum. Once the energy E is determined, the force balance equations at each point i are the minimization conditions

$$\partial E/\partial \boldsymbol{u}(\boldsymbol{i}) = 0. \tag{A13}$$

For the quadratic energy described above, the derivative in

Eq. (A13) is a linear function of $\boldsymbol{u}(\boldsymbol{i}')$ over values of i' that are equal to, nearest neighbors of, or next-nearest neighbors of $\boldsymbol{i}$. The coefficients can be exactly determined as a finite difference of E with respect to $\boldsymbol{u}(\boldsymbol{i})$ and $\boldsymbol{u}(\boldsymbol{i}')$. Then a linear equation solver is used to find $\boldsymbol{u}$ by solving Eq. (A13). This procedure does not require analytic determination of the force balance equation, which is an advantage because the analysis has many different cases.[27]

[1] E. Bauer, Z. Kristallogr. **110**, 372 (1958).

[2] D. Leonard, M. Krishnamurthy, C. M. Reaves, S. P. DenBaars, and P. M. Petroff, Appl. Phys. Lett. **63**, 3203 (1993); J. M. Moison, F. Houzay, F. Barthe, and L. Leprince, *ibid.* **64**, 196 (1994); A. Madhukar, Q. Xie, P. Chen, and A. Konkar, *ibid.* **64**, 2727 (1994); R. Leon, T. J. Senden, Y. Kim, C. Jagadish, and A. Clark, Phys. Rev. Lett. **78**, 4942 (1997); Y. Ebiko, S. Muto, D. Suzuki, S. Itoh, K. Shiramine, T. Haga, Y. Nakata, and N. Yokoyama, *ibid.* **80**, 2650 (1998).

[3] W. K. Burton, N. Cabrera, and F. C. Frank, Philos. Trans. R. Soc. London, Ser. A **243**, 299 (1951).

[4] J. A. Venables, G. D. T. Spiller, and M. Hanbucken, Rep. Prog. Phys. **47**, 399 (1984).

[5] J. D. Weeks and G. H. Gilmer, Adv. Chem. Phys. **40**, 157 (1979); S. Clarke and D. D. Vvedensky, Phys. Rev. Lett. **58**, 2235 (1987); A. Madhukar and S. V. Ghaisas, CRC Crit. Rev. Solid State Mater. Sci. **14**, 1 (1988); H. Metiu, Y.-T. Lu, and Z. Y. Zhang, Science **255**, 1088 (1992); H. C. Kang and W. H. Weinberg, J. Chem. Phys. **90**, 2824 (1989).

[6] C. Ratsch and A. Zangwill, Surf. Sci. **293**, 123 (1993).

[7] C. Ratsch, P. Šmilauer, D. D. Vvedensky, and A. Zangwill, J. Phys. I **6**, 575 (1996).

[8] H. M. Koduvely and A. Zangwill, Phys. Rev. B **60**, R2204 (1999).

[9] F. K. LeGoues, Mater. Res. Bull. **21**, 38 (1996); B. A. Joyce, J. L. Sudijono, J. G. Belk, H. Yamaguchi, X. M. Zhang, H. T. Dobbs, A. Zangwill, D. D. Vvedensky, and T. S. Jones, Jpn. J. Appl. Phys. **36**, 4111 (1997).

[10] V. A. Shchukin and D. Bimberg, Rev. Mod. Phys. **71**, 1125 (1999).

[11] M. Schneider, I. K. Schuller, and A. Rahman, Phys. Rev. B **36**, 1340 (1987); M. H. Grabow and G. H. Gilmer, Surf. Sci. **194**, 333 (1988); B. W. Dodson, CRC Crit. Rev. Solid State Mater. Sci. **16**, 115 (1990).

[12] A. Kobayashi, S. M. Paik, and S. Das Sarma, J. Vac. Sci. Technol. B **6**, 1145 (1988); D. A. Faux, G. Gaynor, C. L. Carson, C. K. Hall, and J. Bernholc, Phys. Rev. B **42**, 2914 (1990); B. G. Orr, D. Kessler, C. W. Snyder, and L. Sander, Europhys. Lett. **19**, 33 (1992); A. Madhukar, J. Cryst. Growth **163**, 149 (1996).

[13] D. A. Faux, G. Gaynor, C. L. Carson, C. K. Hall, and J. Bernholc, Phys. Rev. B **42**, 2914 (1990); J. Kew, M. R. Wilby, and D. D. Vvedensky, J. Cryst. Growth **127**, 508 (1993); F. Much, M. Ahr, M. Biehl, and W. Kinzel, Europhys. Lett. **56**, 791 (2001).

[14] B. J. Spencer, P. W. Voorhees, and S. H. Davis, Phys. Rev. Lett. **67**, 3696 (1991); B. J. Spencer, P. W. Voorhees, and S. H. Davis, J. Appl. Phys. **73**, 4955 (1993); B. J. Spencer, S. H. Davis, and P. W. Voorhees, Phys. Rev. B **47**, 9760 (1993).

[15] P. Politi, G. Grenet, A. Marty, A. Ponchet, and J. Villain, Rep. Prog. Phys. **324**, 271 (2000).

[16] M. Born and K. Huang, *Dynamical Theories of Crystal Lattices* (Oxford University Press, Oxford, 1954).

[17] M. Ortiz and R. Phillips, Adv. Appl. Mech. **36**, 1 (1999).

[18] V. K. Tewary, Adv. Phys. **22**, 757 (1973).

[19] V. S. Stepanyuk, D. I. Bazhanov, W. Hergert, and J. Kirschner, Phys. Rev. B **63**, 153406 (2001).

[20] C. Priester and M. Lannoo, Phys. Rev. Lett. **75**, 93 (1995).

[21] L. G. Wang, P. Kratzer, N. Moll, and M. Scheffler, Phys. Rev. B **62**, 1897 (2000).

[22] J. M. Rickman and D. J. Srolovitz, Surf. Sci. **284**, 211 (1993).

[23] K. H. Lau and W. Kohn, Surf. Sci. **65**, 607 (1977).

[24] P. Peyla, A. Vallat, C. Misbah, and H. Muller-Krumbhaar, Phys. Rev. Lett. **82**, 787 (1999).

[25] Y. Saito, H. Uemura, and M. Uwaha, Phys. Rev. B **63**, 045422 (2001).

[26] L. D. Landau and E. M. Lifschitz, *Theory of Elasticity* (Pergamon, Oxford, 1970).

[27] R. E. Caflisch and C. Connell (unpublished).

[28] J. Tersoff, Y. H. Phang, Z. Zhang, and M. G. Lagally, Phys. Rev. Lett. **75**, 2730 (1995).

[29] R. V. Kukta and K. Bhattacharya, Thin Solid Films **357**, 35 (1999).

[30] D. J. Srolovitz (private communication).

[31] I. Daruka, A.-L. Barabási, S. J. Zhou, T. C. Germann, P. S. Lomdahl, and A. R. Bishop, Phys. Rev. B **60**, R2150 (1999).

[32] We use the notation m_0, m_1, etc. to represent coefficients of the monopole, dipole, etc., respectively. The numbering is meant to represent the power of x in the denominator of the single-step term.

[33] V. I. Marchenko and A. Ya. Parshin, Sov. Phys. JETP **52**, 129 (1980).

[34] J. Stewart, O. Pohland, and J. M. Gibson, Phys. Rev. B **49**, 13 848 (1994).

[35] V. I. Marchenko, JETP Lett. **33**, 381 (1981).

[36] O. L. Alerhand, D. Vanderbilt, R. D. Meade, and J. D. Joannopoulos, Phys. Rev. Lett. **61**, 1973 (1988).

[37] P. N. Keating, Phys. Rev. **145**, 637 (1966).

[38] R. M. Martin, Phys. Rev. B **1**, 4005 (1970).

[39] F. Grosse and J. Neugebauer, Phys. Rev. B **63**, 085207 (2001).

[40] S. Osher and J. A. Sethian, J. Comput. Phys. **79**, 12 (1988); S. Chen, B. Merriman, S. Osher, and P. Smereka, *ibid.* **135**, 8 (1997).

[41] M. F. Gyure, C. Ratsch, B. Merriman, R. E. Caflisch, S. Osher, J. J. Zinck, and D. D. Vvedensky, Phys. Rev. E **58**, R6927 (1998).

[42] W. Seifert, N. Carlsson, M. Miller, M.-E. Pistol, L. Samuelson, and L. R. Wallenberg, Prog. Cryst. Growth Charact. **33**, 423 (1996).

[43] C. Ratsch, M. F. Gyure, S. Chen, M. Kang, and D. D. Vvedensky, Phys. Rev. B **61**, R10 598 (2000).

[44] C. Ratsch, A. P. Seitsonen, and M. Scheffler, Phys. Rev. B **55**, 6750 (1997).

[45] F. Gutheim, H. Muller-Krumbhaar, and E. Brener, Phys. Rev. E **63**, 041603 (2001).

[46] C. Ratsch, A. Zangwill, and P. Smilauer, Surf. Sci. **314**, L937 (1994).

[47] M. Meixner, E. Scholl, V. A. Shchukin, and D. Bimberg, Phys. Rev. Lett. **87**, 236101 (2001).

[48] Q. Xie, A. Madhukar, P. Chen, and N. P. Kobayashi, Phys. Rev. Lett. **75**, 2542 (1995).

[49] J. Tersoff, C. Teichert, and M. G. Lagally, Phys. Rev. Lett. **76**, 1675 (1996).

[50] A. Madhukar, Thin Solid Films **231**, 8 (1993).